Research on Engineering Structures and Materials

VOLUME 10 ISSUE 1 FEBRUARY 2024

Corrosion effects on axial compressive behavior of steel strapping tensioning technique-confined concrete

Yong-Zheng Goh, Kee-Hong Ler, Chee-Loong Chin, Chau-Khun Ma, Hongtao Su, Abdillah Sani bin Mohd Najib

To cite this article

Goh YZ, Ler KH, Chin CL, Ma CK, Su H, Najib ASBM. Corrosion effects on axial compressive behavior of steel strapping tensioning technique-confined concrete. *Res. Eng. Struct. Mater*., 2024; 10(2): 801-817.

Disclaimer

All the opinions and statements expressed in the papers are on the responsibility of author(s) and are not to be regarded as those of the journal of Research on Engineering Structures and Materials (RESM) organization or related parties. The publishers make no warranty, explicit or implied, or make any representation with respect to the contents of any article will be complete or accurate or up to date. The accuracy of any instructions, equations, or other information should be independently verified. The publisher and related parties shall not be liable for any loss, actions, claims, proceedings, demand or costs or damages whatsoever or howsoever caused arising directly or indirectly in connection with use of the information given in the journal or related means.

Research Article

Corrosion effects on axial compressive behavior of steel strapping tensioning technique-confined concrete

Yong-Zheng Goh[*1,a], Kee-Hong Ler[1], Chee-Loong Chin[1,b], Chau-Khun Ma[1,2], Hongtao Su[3], Abdillah Sani bin Mohd Najib[4,c]

[1]*Faculty of Civil Engineering, Universiti Teknologi Malaysia, Malaysia*
[2]*Forensic Engineering Centre, Institute of Smart Infrastructure and Innovative Construction, Faculty of Civil Engineering, Universiti Teknologi Malaysia, Malaysia*
[3]*China Communication 2nd Navigational Bureau 2nd Engineering Co., Ltd., China*
[4]*Faculty of Mechanical Engineering, Universiti Teknologi Malaysia, Malaysia*

Article Info	Abstract
	This paper presents an experimental study on effect of corrosion on durability performance of circular Steel Strapping Tensioning Technique (SSTT)-confined concrete tested under uniaxial compression. A total of 13 specimens, including 11 confined specimens and 2 plain specimens were tested in this study. The main parameters were prestressing level and corrosion protection. Corrosion was simulated through impressed current accelerated corrosion technique. The experimental results indicated that influence of corrosion was insignificant on peak strength and slight reduction in deformation ability to corroded circular SSTT-confined concrete under low corrosion severity. It was observed that Zn-Al-Cd ingot and long-oil alkyd paint coating shows good protection ability, while 6061 aluminum alloy and 99.9% pure magnesium is not suitable to be used as corrosion protection system. Based on regression analysis, prediction models for peak stress and peak strain for circular corroded SSTT-confined concrete were proposed.

1. Introduction

Existing concrete structures eventually reached their designated service life and deteriorated in structural performance. Strengthening of these structures through retrofitting techniques are more practical solutions than demolishing and replacing with new one. An alternative retrofitting technique with increasing attention is Steel Strapping Tensioning Technique (SSTT) originated from packaging industry. SSTT involved externally pre-tensioning of steel strap on concrete to provide confining effect. Numerous studies revealed that SSTT is an effective confinement method in enhancing concrete properties including strength [1, 2] and deformation ability [3, 4]. Moghaddam *et al.* [1] noticed that by increasing numbers of strap layers significantly enhanced the ultimate strength of confined concrete. Chin *et al.* [4] reported that with application of SSTT, the confined concrete able to achieve ductile post-peak behavior. It was also proven that SSTT able to rehabilitate damaged concrete structures, returning to its original strength [5-7]. Mohd Apandi *et al.* [7] proven the ability of SSTT to rehabilitate the strength and ductility of damaged concrete structure, delaying its damage by increasing the ultimate strain. Nevertheless, SSTT also possess the advantage of flexibility in design [8]. Lee *et al.* [8] noticed that by adjusting the prestressing level on steel strap will affect both strength and ductility of confined concrete.

Despite the remarkable performance of SSTT-confined concrete, the studies on its durability performance are very limited. In composite structures involving the application of steel, corrosion as an inevitable factor influencing its performance to be considered in design. It is a known fact that corrosion induced loss in effective cross-sectional area of steels and resulted in deterioration of its mechanical performance [9]. Furthermore, corrosion extent resulted in degradation of steel with respect of time and transforming it from ductile into brittle manner, increasing the possibility of sudden rupture failure [10]. Concrete structures retrofitted by steel confinement relies on the composites effect between two materials. Corrosion of steel confinement will deteriorate the structural performance of confined concrete [11-13]. Han et al. [11] concluded that deterioration mechanism of corroded external steel confined concrete depends on two aspects, i.e., reduction in sectional area of steel resulted in decrease in strength of steel confinement and reduction of confining effect on concrete leads to decrease in strength of concrete and deformation ability of confined concrete. Previous study reported by Lee et al. [14] shows no significant deterioration in strength for SSTT-confined concrete up to 3 months of natural exposure. However, the corrosion was insignificant due to the fact that corrosion in actual environment generally take up to years [15]. Furthermore, the designated service life for structures is usually 50 years and above. Hence, this short period of exposure is unable to represent the full-service life of structures. Moreover, the influence of corrosion on SSTT-confined concrete was not thoroughly discussed in his studies. Therefore, more comprehensive experimental studies are required.

This paper attempt to study the effect of corrosion on the behavior of circular SSTT-confined concrete. The experimental results for corroded circular SSTT-confined concrete tested under uniaxial compression is presented. The main parameters included prestressing level and corrosion protection. The corrosion in this study is simulated by impressed current accelerated corrosion technique through immersion in NaCl solutions. The performance of the corroded specimens was then evaluated through their stress-strain curve and failure mode.

2. Experimental Program

2.1. Specimens Preparation and Material Properties

The mix proportion for concrete was prepared with CEM 1 42.5N cement in accordance to BS EN 206-1 [16] as shown in Table 1. Tap water was used to prepare the concrete mix. 10 mm maximum nominal size crushed coarse aggregate and well-graded river sand for fine aggregate was used. Compression tests were carried out according to BS EN 12390-3:2009 [17] after 28 days of curing on three 100 mm × 100 mm × 100 mm concrete cubes. The average compressive stress, $f_{cu,ave}$ is 46.4 MPa. The cylindrical strength of concrete, f'$_c$ was determined to be 34.5 MPa. Note that the value of f_c is taken as unconfined concrete strength, f_{co} in this study as the specimens used were in cylindrical shape.

Table 1. Concrete mix proportion for normal strength concrete

Cement (kg/m³)	Fine Aggregate (kg/m³)	Coarse Aggregate (kg/m³)	Water (kg/m³)
432	842	825	233

Steel strap used for confinement is made of low-cost recycled steel, which commonly used in packaging industry. The nominal thickness (*t*) and width (*w*) were 0.5 mm and 16 mm, respectively. Tensile tests were performed to identify its material properties in accordance to ISO 6892:2019 [18]. Universal Testing Machine (UTM) with load cell of 250 kN was used to carried out the test. 40 mm in length of steel strap were prepared. **Fig. 1** shows the stress-strain curves for tensile tests. The yield strength *(f*$_y$) is 735 MPa; the ultimate

strength (f_u) is 753 MPa, the ultimate strain (ε_u) is 0.0070 and the elastic modulus (E) is 220 GPa.
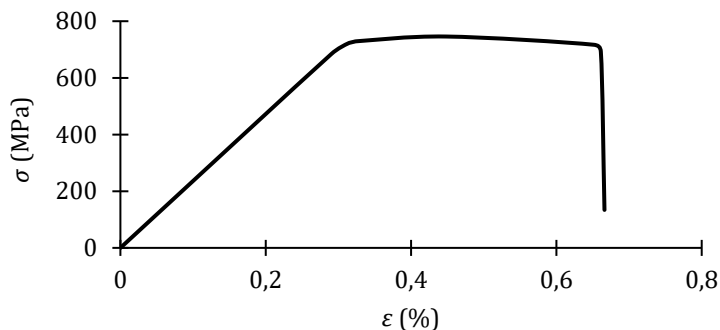

Fig. 1. Stress-strain curve of steel strap

The confinement technique involved the use of pre-tensioning of steel straps around the specimens. Steel straps were cut into desired lengths and formed into steel hoops. The length of internal and external anchorage was set to 50 mm. The specimens were confined by these steel straps using PT-52 pneumatic tensioner and secured in place using two self-regulated end clips [19, 20]. These end clips enabled multiple layers of steel straps to regulate themselves and avoid early loss of pre-tensioned force. The steel straps were tensioned around the specimens with constant air pressure of 0.25 MPa and 0.35 MPa. Consistent value of tensioning pressure secures the effective utilization of steel straps and avoids early crushing of confined concrete. The spacings between steel straps (s) were fixed at 14.4 mm along the middle section. Both end regions of the specimens were confined by two steel straps with closer spacing to avoid premature failure during compression tests. Fig. 2 shows the confinement steel straps, self-regulated end clips, and configurations for confined concrete.
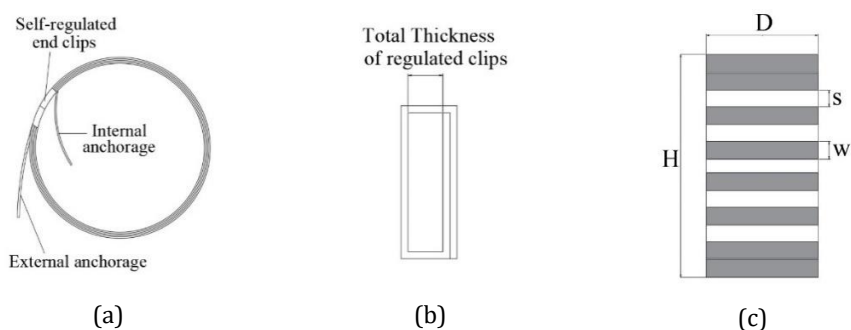

(a)   (b)   (c)

Fig. 2. Schematic diagram: (a) steel hoop confinement; (b) self-regulated end clips; and (c) SSTT-confined concrete

2.2. Application of Corrosion Protection System

The corrosion protection system applied were sacrificial anode cathodic protection (SACP) and paint coatings. The sacrificial anodes used included 6061 aluminum alloy rod, 99.9% pure magnesium rod and Zn-Al-Cd alloy ingot. Both rods were with dimensions of 90 mm and 16 mm in length and diameter, respectively. The zinc alloy ingot in dimensions of 30 mm × 80 mm × 140 mm in thickness, width, and length, respectively. Before connecting to

the specimens, all the sacrificial anodes were sanded to remove any existing oxides. As each of the consecutive steel hoops confined on the concrete were separated, a copper wire is used to connect all the steel straps to the sacrificial anode. This is to ensure the protection ability to reach all the steel straps. The potential differences between the steel strap and sacrificial anodes were measured using digital multimeter. Table 2 shows the results of the measured potential differences.

Table 2. Potential differences between steel strap and sacrificial anodes.

Sacrificial Anode	Potential Difference (V)
6061 Aluminium Alloy	-0.154
Zn-Al-Cd Alloy	-0.445
Pure Magnesium	-1.167

The paint coatings used was long oil alkyd paint (OAP) with percentage volume solid of 60%. Prior to pre-tensioning work, all the steel straps were degreased with thinner to remove oil contaminant initially on the steel surface. This is to ensure a reliable test results and good adhesion between paint coatings and steel surface. Full coverage coating including exposed concrete surface and the end clips were painted. The thickness of dry firm was controlled to approximately 50 μm with single layer of coating. To achieve this, the wet firm thickness of coating is carefully controlled to approximate 85 μm by using comb gauge and a thickness control device. The freshly coated specimen was left to dry for 3 days in room temperature.

2.3. Nomenclature of Specimens

A total of 13 concrete cylinder specimens with 100 mm and 200 mm in diameter (D) and height (H) respectively were prepared. 11 specimens were confined externally with multiple layers of steel straps and 2 plain specimens were set as control specimens.

Table 3. Experimental test results for corroded SSTT-confined concrete specimens.

Specimens ID	Δm (kg)	Δt (mm)	Actual C_d* (%)	Peak Stress (MPa)	f_{cc}/f_{co}	Peak Strain (%)	$\varepsilon_{cc}/\varepsilon_{co}$
C-N-0-0-0	-	-	-	34.5	-	0.24	-
C-N-0-0-2	-0.0050	-	-	39.6	-	0.12	-
C-N-300-1-0	-	-	-	67.7	1.962	1.71	7.125
C-N-500-1-0	-	-	-	71.1	2.061	2.32	9.667
C-N-300-1-2	0.0080	0.019	3.78	67.1	1.945	1.17	4.875
C-N-500-1-2	0.0105	0.025	4.96	67.7	1.962	1.27	5.292
C-Al-300-1-2	0.0110	0.026	5.20	60.7	1.759	1.50	6.250
C-Al-500-1-2	0.0115	0.027	5.44	63.4	1.838	1.67	6.958
C-Mg-300-1-2	0.0075	0.015	3.55	63.4	1.838	1.08	4.500
C-Zn-300-1-2	0.0040	0.009	1.89	72.3	2.096	1.71	7.125
C-OAP-300-1-2	0.0010	0.002	0.47	64.4	1.867	0.66	2.750

*$Corrosion\ degree, C_d = \frac{\Delta t}{t} \times 100\%$

The specimens were labelled as follows: C-a-b-c-d. C indicated the circular concrete specimens; a, the corrosion protection applied; b, the prestressed value according to strength of steel strap; c, the thickness of confinement; d, the durations of immersion in corrosion test. For example, C-Al-300-1-2 indicated normal strength concrete specimens wrapped using steel straps protected by 6061 aluminum alloy rods. Also, the specimen was confined by prestressed value of 300 MPa with 2 layers of straps. The specimen was immersed in corrosion test for 2 hours. Other details of specimens are listed in Table 3.

2.4. Test Setup

In first stage, the confined concretes were immersed in salt solution for a designed period to allow development of corrosion. Impressed current accelerated corrosion test was adopted to simulate the corrosion environment. The test setup mainly consists of container, electrolytic solution, and direct current (D.C.) power supply. The electrolytic solution formed with 3.5% sodium chloride (NaCl) by the weight of water. The positive pole of the D.C. power supply was connected to the steel straps of the tested specimen, which acted as an anode. The negative pole of the power source was connected to a stainless-steel rod, which acted as a cathode. The corrosion degree, C_d was designed to be 5%, which was controlled by current densities of 9400 μA cm^{-2} (5 A of fixed current) based on Faraday's Law in electrochemistry. Immersion durations for specimens to be corroded is set to be consistent for 2 hours. To ensure the consistency of corrosion development, the salt solutions was renewed every hour. Besides, the current supplied is consistently observed and adjusted to maintain at 5 A throughout the test. Fig. 3 shows an example of setup for the test. Upon termination of corrosion test, the specimens were left to dry in room temperature for 2 days before proceeding for corrosion product cleaning based on ISO 8407 [21]. The corrosion products were removed by applying dilute hydrochloric acid (HCl), subsequently removed by non-abrasive brush, and rinsed with clean water. The cleaned specimens were then left to dry in room temperature for 1 day. Weight loss method was used to identify the mass loss due to corrosion, Δm. Subsequently, the mass loss data were converted to thickness loss, Δt based on density of 7.86 g cm^{-3} for steel straps. To ensure that the weight of concrete is not affected by the immersion, a plain concrete was used and repeated with similar procedures as above.

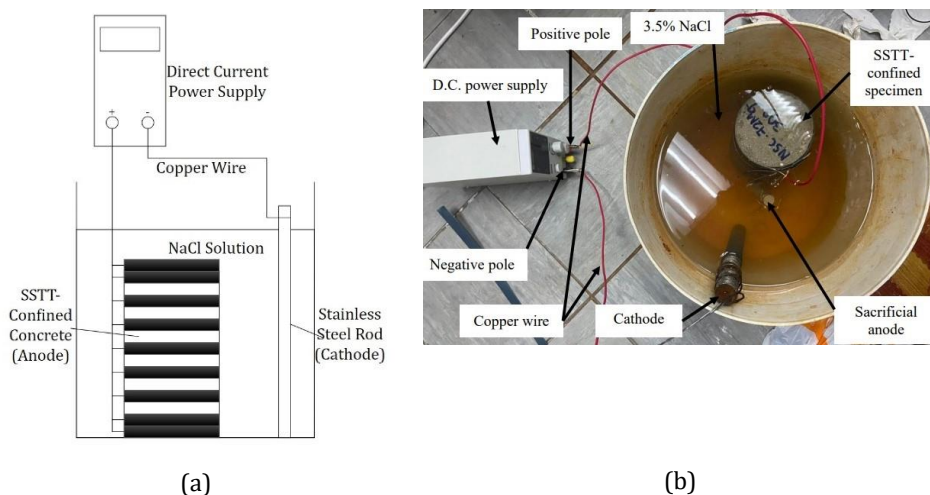(a)   (b)

Fig. 3. Corrosion test setup: (a) schematic diagram; and (b) actual configuration

In second stage, the specimens were tested under uniaxial compression after completion for corrosion test. Load and deformations were used to investigate the influence of corrosion on the behavior of corroded specimens. A 2000 kN capacity hydraulic Tinius Olsen Super "L" UTM was adopted to perform the compression test. All the tests were carried out under displacement control with a rate of 0.006 mm/s. A total of three linear variable differential transducers (LVDTs) were mounted to measure the axial deformation. The LVDTs were installed on the holder rig at three different directions parallel to the tested specimens. The increments of load were measured using a built-in machine load

cell. The load and deformations were recorded for every second until failure with data logger. Fig. 4 shows the test setup for compressions test.
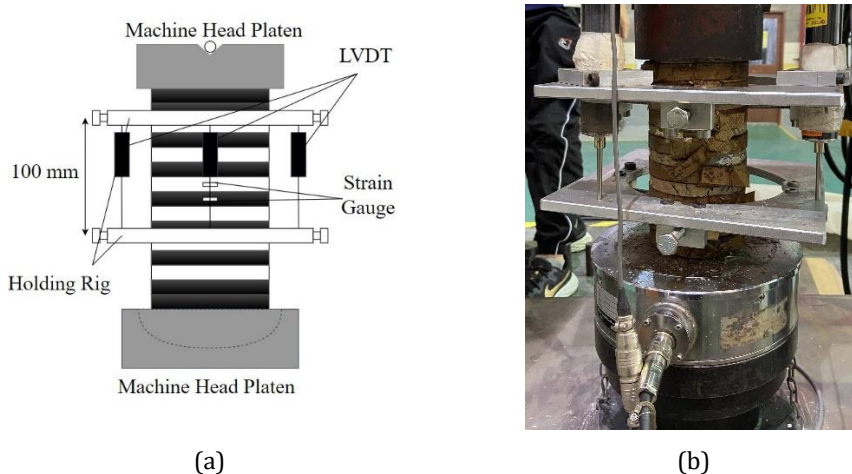

(a)   (b)

Fig. 4. Axial compression test setup: (a) schematic diagram; and (b) actual configuration.

3. Results and Discussion

3.1. Evaluation of Corrosion Degree

The mass of before and after 2 hours immersion in salt solution for C-N-0-0-2 was recorded as shown in Table 3. Results indicated a negligible increment in weight after immersion. This indicated that the use of weight loss method for calculation of corrosion degree is appropriate.

Based on the theoretical calculations using Faraday's Law in electrochemistry, the predicted corrosion degree is expected to be 5%. However, corrosion degree for C-N-300-1-2 exhibited a lower corrosion degree. In fact, considering the influence for combination of prestressing force and corrosion on the steel strap, the actual corrosion degree was expected to be higher than the theoretical value [22]. Higher prestressing force leads to formation of microcracks on the surface of steel straps. These microcracks acted as site for initiation of corrosion, which increased the rate of development of corrosion. This can be proven that the C-N-500-1-2 exhibited higher corrosion degree under similar conditions. The discrepancy between actual and theoretical corrosion degree can be attributed to the presence of dark blue metallic coating disrupted the development of corrosion. During the corrosion process, two major substances were observed, as shown in Fig. 5 (b). It can be observed that the dark blue substance formed solids around the cathode, which supported that it is metallic. Furthermore, this can be supported by the observation that the dark blue metallic coating fully disappeared after the corrosion test, as shown in Fig. 5 (a) and (c). This phenomenon also explained the observations in study conducted by Lee et al. [14]. This confirmed that the presence of dark blue metallic coating delayed the development of corrosion process for steel substrate. The metallic coating acted similarly with the protection mechanism of SACP.
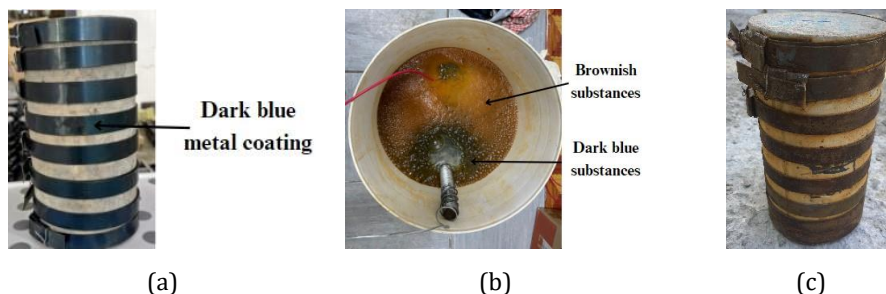
Fig. 5. Observations for conditions: (a) before corrosion; (b) during corrosion; and (c) after corrosion

It is unexpected that the corrosion degree of C-Mg-300-1-2, C-Al-300-1-2 and C-Al-500-1-2 were similar to or higher than the unprotected specimens. By visual inspection, these specimens displayed similar corrosion severity as the unprotected specimens as shown in Figure 6. This indicated that 6061 aluminum alloy and 99.9% pure magnesium rod could not provide sufficient protection to the steel straps under corrosive environments. In comparison with C-Zn-300-1-2 and C-OAP-300-1-2, both exhibited lower corrosion degree. Based on Table 2, the potential differences between SACP and steel straps suggested that Zn-Al-Cd alloy should provide lower protection ability than 99.9% pure Mg. However, the results indicated a contradiction with the expectation. This can be attributed to the size of Zn-Al-Cd alloy ingot is larger than Mg rod. The protection ability of sacrificial anode is highly dependent on its size. The larger Zn-Al-Cd alloy provide wider coverage of protection ability to the steel straps compared to Mg rod. Among all of the corrosion protection system adopted, OAP exhibited greatest protection ability with corrosion degree of 0.49%, followed by Zn-Al-Cd alloy with 1.89% and 99.9% pure magnesium with 3.55%, and the least is 6061 aluminum alloy with more than 5%.
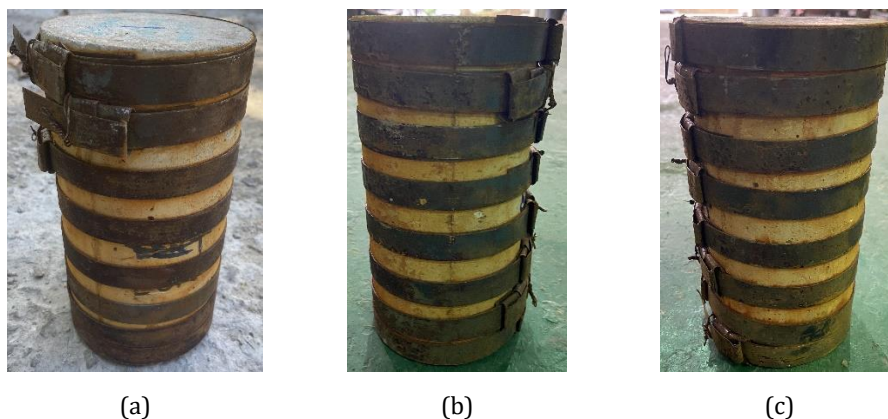

Fig. 6. Observations for corroded specimens: (a) unprotected; (b) Mg; and (c) Al

3.2. Failure Mode

For unconfined specimens, the failure mode was generally in the form of sudden shear splitting as shown in Fig. 7 (a). The specimens exhibited a brittle behavior as the load carrying capacity reduced drastically after ultimate capacity. The cracks initially formed at diagonal of the top part and extended towards the opposite diagonal of the bottom part. Both unconfined specimens failed with a cracking sound upon reaching their peak

strength. For uncorroded confined specimens confined with two-layer steel straps, there was no cracks formed at the initial stage of compression tests. Some distinct crisp metal screeching sounds exhibited when the load applied exceed the concrete strength. The formation of microcracks initiated at the middle section of the confined concrete with some minor cracking sound. These cracks continue to extend towards bottom direction as the load increased. Upon failure, a loud explosive sound was heard as an effect of the steel strap confinement at the middle section ruptured. It was observed that the middle part of C-N-300-1-0 experienced failure in crushing as shown in Fig. 7 (b). However, the existence of steel straps confinement effectively prevented the concrete from falling apart. Different from C-N-300-1-0, the core concrete split into two sections for C-N-500-1-0 as shown in Fig. 7 (c). Both concrete and steel strap were observed that they fractured simultaneously.
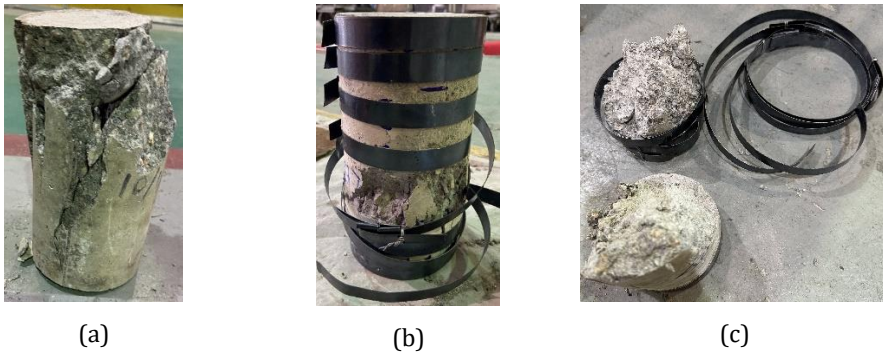

(a) (b) (c)

Fig. 7. Failure mode: (a) C-N-0-0-0; (b) C-N-300-1-0; and (c) C-N-500-1-0

Among all the corroded confined specimens with and without protection, only C-N-500-1-2 experienced failure in a loud explosive sound and fracture of steel strap confinement in the middle section as shown in Fig. 8 (a). A severe crushing of concrete was observed but the corroded steel strap confinement still remained its effectiveness in preventing the falling of concrete. For other specimens in this series, the failure occurred in most cases due to the crushing of concrete along the middle section without snapping of steel straps confinement as shown in Fig. 8 (b) - (f). In general, it was observed that all the specimens in this series behaved in a ductile manner after reaching their ultimate capacity. The influence of corrosion with low severity on the failure mode were not significant for all corroded confined specimens.
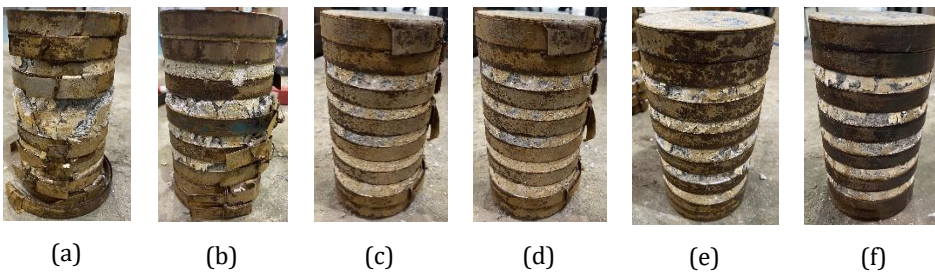

(a) (b) (c) (d) (e) (f)

Fig. 8. Failure mode: (a) C-N-500-1-2; (b) C-N-300-1-2; (c) C-Al-300-1-2; (d) C-Al-500-1-2; (e) C-Mg-300-1-2; and (f) C-Zn-300-1-2.

3.3. Stress-Strain Behavior

The peak stress of specimens obtained from compression tests were presented in Table 3. The unconfined concrete strength, f_{co} of C-N-0-0-0 was 34.5 MPa, which displayed a variation compared to C-N-0-0-2 with 39.6 MPa. The difference in value between before and after immersion is believed to be statistical variations of strength values, inherently exhibited a level of variability. Chloride content in NaCl solutions will not affect the strength of core concrete as there is no internal reinforcement involved in this study. Moreover, the strength development of concrete due to hydration process gradually drops and required longer time to observe a clear variation in strength [23].

Fig. 9 shows the stress-strain curve for corroded specimens without protection. In these figures, the axial deformations were obtained from average readings of LVDTs. From Fig. 9, it can be observed that corrosion has insignificant impact on the load-carrying capacity of the confined specimens. The peak stress of C-N-300-1-2 and C-N-500-1-2 were 67.1 MPa and 67.7 MPa, respectively. Compared to C-N-300-1-0 and C-N-500-1-0, the reduction in peak stress under the influence of corrosion were as low as 0.94% and 4.66% respectively. Besides, it can be observed that C-N-500-1-2 with higher corrosion degree (4.96%) shows higher reduction in its peak stress. It is as expected that higher corrosion degree of steel straps confinement resulted in lower peak stress of the confined specimens. Nevertheless, this finding suggested that SSTT-confined concrete shows the ability to preserve well for its peak stress under low corrosion severity. However, the influence of corrosion shows greater effects on the deformation ability of the confined concrete. It can be observed that in overall, the corroded specimens behaved in a less ductile manner. Both C-N-300-1-2 and C-N-500-1-2 achieved its peak stress with lower strain. Corrosion reduced the effective cross-sectional area of steel straps confinement, thus reducing its mechanical properties. This in turns resulted in reduction for its confinement effect.
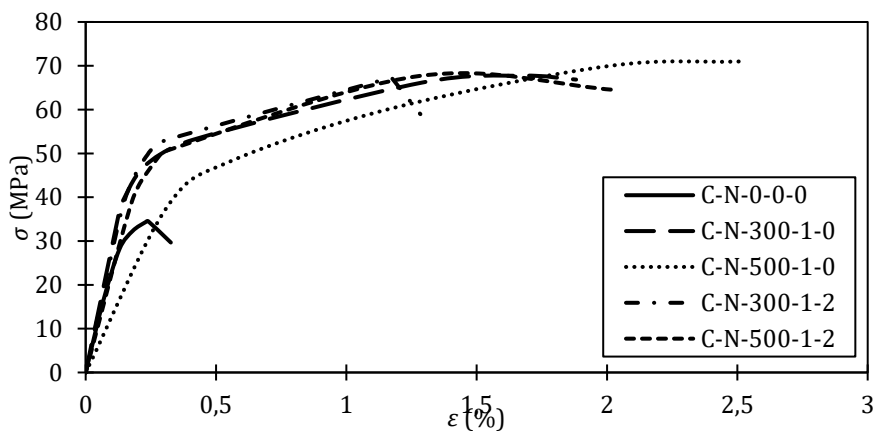

Fig. 9. Stress-strain behaviour of unprotected corroded specimens

Fig. 10 presented the stress-strain curve for specimens with protection. From the figure, it can be observed that C-Al-300-1-2 and C-Al-500-1-2 exhibited lower peak stress and deformation compared to C-N-300-1-2 and C-N-500-1.2. These specimens exhibited higher corrosion degree which consistent with previous expectation. For C-Mg-300-1-2, its corrosion degree (3.55%) was similar to C-N-300-1-2 (3.78%). The reduction in peak stress and deformation were approximately similar. Hence, it can be concluded that 6061 aluminum alloy and 99.9% pure magnesium are not suitable to be used as sacrificial anode for steel straps confinement. Compared to C-Zn-300-1-2 and C-OAP-300-1-2 with lower

corrosion degree of 1.89% and 0.49% respectively, both protections proven their ability to maintain their strength and deformation ability under influence of corrosion.
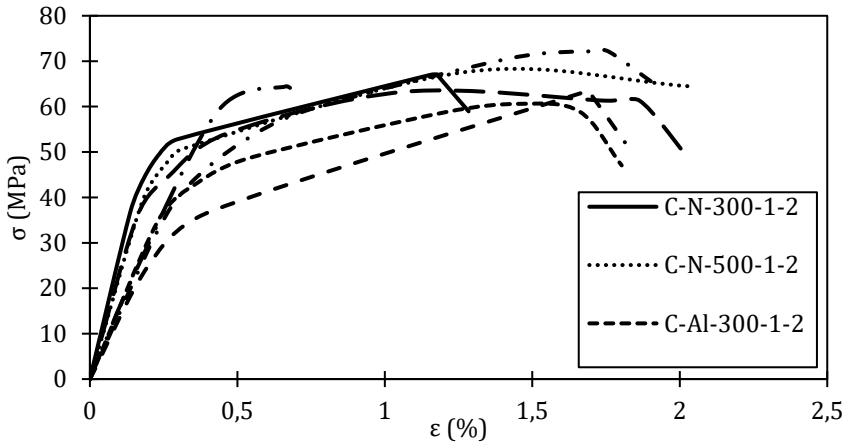

Fig. 10. Stress-strain behaviour for protected corroded specimens

4. Model Assessment for Corroded Circular SSTT-Confined Concrete

4.1. Modification on Existing Confinement Models

In this section, the experimental results in this study will be assessed with current existing confinement models. The assessment will be carried out based on performance in prediction for peak stress and peak strain. To the author's best knowledge, currently there is no study attempted to propose confinement model that account the effect of corrosion for SSTT-confined concrete. In this regard, a series of models for SSTT-confined concrete were collected from existing literature as presented in Table 4. These models were modified to account the effects of corrosion as discussed below.

Studies revealed that confining pressure, f_l acting on concrete evidently affected the behavior of confined concrete. In the case of steel-confined concrete, f_l is generated from hoop tension, F_h in steel, which can be evaluated as Eq (1) below:

$$F_h = t f_y w s \tag{1}$$

For partial-steel confined concrete, f_l can be calculated through Eq (2) proposed by Moghaddam *et al.* [24]:

$$f_l = \frac{2tf_y}{D}\left(\frac{w}{w+s}\right) \tag{2}$$

where, D is diameter of concrete; w is width of steel strap; and s is clear spacing between confinement hoops. As the effect of corrosion could be directly evaluated based on thickness loss of steel confinement, hence the thickness, t in Eq (2) is modified and replaced with effective thickness, t_e, which can be calculated based on Eq (3):

$$t_e = t - \Delta t \tag{3}$$

Zhang *et al.* [25] recommended that for modelling corroded external steel confined concrete, the influence of corrosion on yield strength of steel confinement should be accounted. Hence, the equation to determine yield strength of corroded steel confinement from Zhang *et al.* [25] is adopted as shown in Eq (4):

$$f'_y = f_y(1 - 1.58C_d) \tag{4}$$

where, f'_y is yield strength of corroded steel confinement. Combining both Eq (3) and Eq (4), confining pressure considering effect of corrosion, f_l can be calculated by Eq (5):

$$f'_l = \frac{2t_e f'_y}{D}\left(\frac{w}{w+s}\right) \tag{5}$$

As listed in Table 4, most of the existing confinement models used concept of reduced confinement effectiveness to account for non-circular shape and spacing. Considering influence of corrosion, combined with Eq (5), effective confinement pressure, f_{le} developed by Sheikh *et al.* [26] can be adopted as:

$$f_{le} = k_e k_s f'_l \tag{6}$$

where, k_e is confinement effectiveness ratio for spacing determined by Eq (7); and k_s is confinement effectiveness ratio for shape determined by Eq (8).

$$k_e = \left(1 - \frac{s}{2D}\right)^2 \tag{7}$$

$$k_s = 1 - \frac{2(D - 2R)^2}{3D^2} \tag{8}$$

where, R is corner radius of square section.

Table 4. Summary of existing models for steel confined concrete

References	fcc/fco Expressions	εcc/εco Expression
Moghaddam et al. [24]	$\frac{f_{cc}}{f_{co}} = 1 + 8\frac{f_{le}}{f_{co}} - 4\left(\frac{f_{le}}{f_{co}}\right)^{1.2}$	$\frac{\varepsilon_{cc}}{\varepsilon_{co}} = \left(\frac{f_{cc}}{f_{co}}\right)^{1.1}$
Awang [27]	$\frac{f_{cc}}{f_{co}} = 2.62\rho_e^{0.4}$ $\rho_e = k_e k_s \rho$	$\frac{\varepsilon_{cc}}{\varepsilon_{co}} = 11.6\rho_e$
Lee et al. [28]	$\frac{f_{cc}}{f_{co}} = 1 + 5.57\frac{f_{le}}{f_{co}}$	$\frac{\varepsilon_{cc}}{\varepsilon_{co}} = 1 + 6.3\frac{f_{le}}{f_{co}}$
Chin et al. [29]	$\frac{f_{cc}}{f_{co}} = 1.124 + 1.02\frac{f_{le}}{f_{co}}$	$\frac{\varepsilon_{cc}}{\varepsilon_{co}} = 0.93 + 1.49\frac{f_{le}}{f_{co}}$
Yang et al. [30]	$\frac{f_{cc}}{f_{co}} = 1 + 3.35k_e k_s\left(\frac{f'_l}{f_{co}}\right)^{0.48}$	-
Proposed model	$\frac{f_{cc}}{f_{co}} = 1 + 5.09\frac{f_{le}}{f_{co}}$	$\frac{\varepsilon_{cc}}{\varepsilon_{co}} = 1 + 27.87\frac{f_{le}}{f_{co}}$

4.2. Performance Assessment

4.2.1 Procedure of Assessment

The performances of existing models in predicting peak stress and peak strain of circular corroded SSTT-confined concrete were evaluated in this section. The performances of each model were assessed by comparison between predicted values with experimental values. Subsequently, the accuracy of each model was analyzed using average absolute error (AAE) and mean square error (MSE) calculated based on Eq (9) and Eq (10), respectively. The reliability of each model was evaluated based on standard deviation (SD) calculated based on Eq (11). Table 5 presented the performances of each model.

$$AAE = \frac{\sum_{i=0}^{n} \left| \frac{mod_i - exp_i}{exp_i} \right|}{N} \tag{9}$$

$$MSE = \frac{\sum_{i=0}^{n} (mod_i - exp_i)^2}{N} \tag{10}$$

$$SD = \sqrt{\frac{\sum_{i=0}^{n} (\frac{mod_i}{exp_i} - \frac{mod_{ave}}{exp_{ave}})^2}{N-1}} \tag{11}$$

Table 5. Summary for performances of existing models

References	Prediction of f_{cc}/f_{co}			Prediction of $\varepsilon_{cc}/\varepsilon_{co}$		
	AAE	MSE	SD	AAE	MSE	SD
Moghaddam *et al.* [24]	0.042	0.008	0.049	0.616	36.258	0.162
Awang [27]	0.310	0.370	0.034	0.608	19.046	0.171
Lee *et al.* [28]	0.054	0.015	0.050	0.602	18.788	0.169
Chin *et al.* [29]	0.318	0.389	0.036	0.777	27.104	0.093
Yang *et al.* [30]	0.232	0.203	0.052	-	-	-
Proposed model	0.041	0.008	0.048	0.309	3.376	0.511

4.2.2 Peak Stress & Proposed Model

Fig. 11 presented the performances of different peak stress models. It clearly illustrated that most of the existing models shows slightly overestimation for peak stress of circular corroded SSTT-confined concrete. The model proposed by Moghaddam et al. [24] shows the highest accuracy with lowest AAE and MSE of 0.042 and 0.008, respectively. However, it tends to overestimate the peak stress when corrosion degree increased. The model proposed by Lee et al. [28] also provided close predictions compared to experimental results. For models proposed by Awang [27] and Chin et al. [29] persistently underestimation of peak stress. In contrast, the model proposed by Yang et al. [30] consistently overestimated the peak stress for circular corroded SSTT-confined concrete.

The influence of corrosion on circular SSTT-confined concrete can be directly evaluated based on thickness loss of steel confinement and reduction on yield strength of steel. Both affected parameters can be reflected in Eq (6). Hence, for current proposed model, a regression analysis is plotted based on measured f_{le}/f_{co} as presented in Fig. 12. Eq (12) is proposed based on the plot and the performance is included in Table 5. It is clearly shown that an overall better performance compared to existing models.

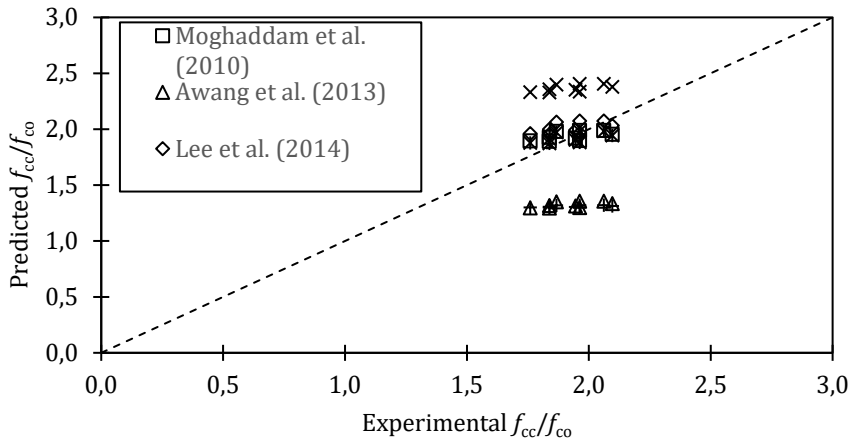$$\frac{f_{cc}}{f_{co}} = 1 + 5.09 \frac{f_{le}}{f_{co}} \tag{12}$$
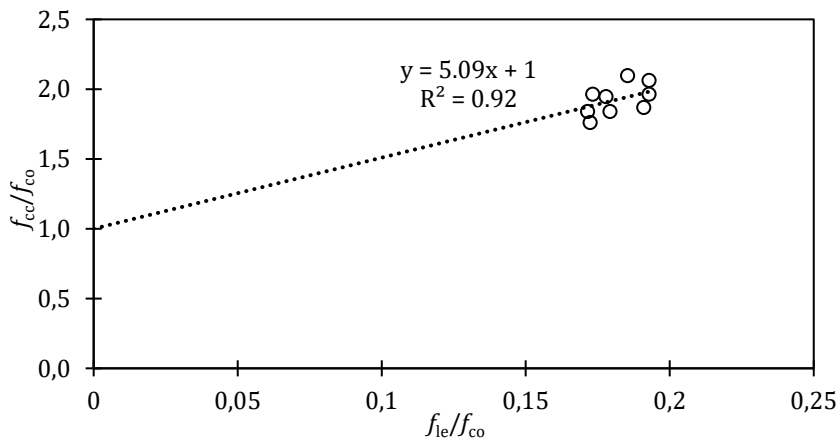
Fig. 11. Performance of peak stress models.

Fig. 12. Performance of proposed peak stress models

4.2.3 Peak Strain & Proposed Model

Fig. 13 presented the performance of each model in estimating peak strain. It can be observed that most of the models underestimated the peak strain of corroded specimens. None of the existing models were capable to provide accurate prediction. In Table 5, the models proposed by Lee et al. [28], Awang [27] and Chin et al. [29] displayed high AAE and MSE. This can be attributed to the fact that these models were empirically derived based on confined high strength concrete (HSC), which generally exhibited lower peak strain due to brittleness problem.

Based on Table 5, it can be observed that most existing models considered effective confining pressure, f_{le} as variable. Hence, a regression analysis is carried out based on measured f_{le}/f_{co} as represented in Fig. 14. Eq (13) is proposed for prediction of peak strain of circular corroded SSTT-confined concrete. From Table 5, the proposed model provided a relatively conservative prediction with AAE and MSE of 0.309 and 3.376, respectively.

$$\frac{\varepsilon_{cc}}{\varepsilon_{co}} = 1 + 27.87 \frac{f_{le}}{f_{co}} \tag{13}$$
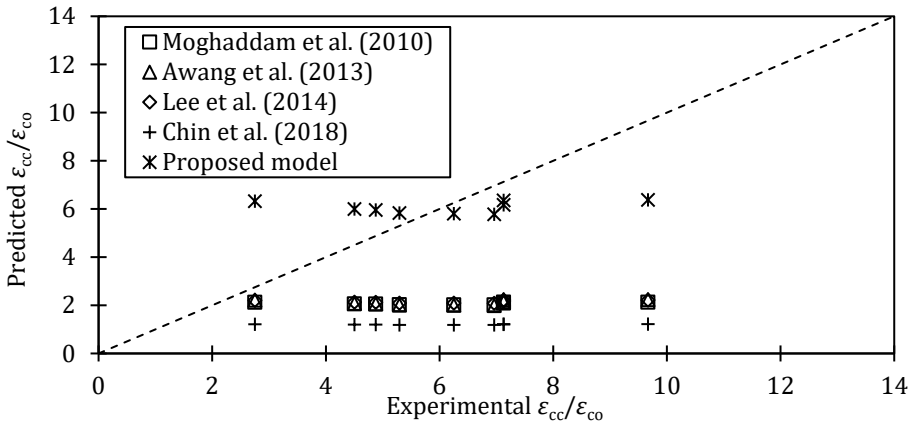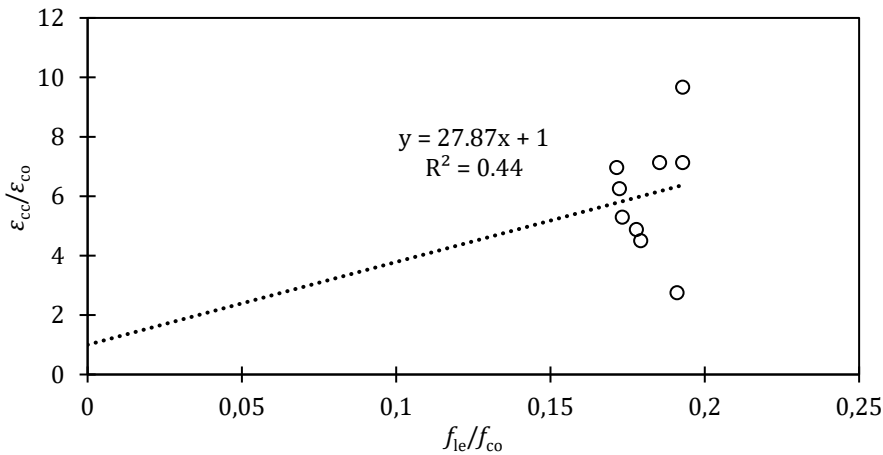
Fig. 13. Performance of peak strain models.

Fig. 14. Performance of proposed peak strain models

5. Conclusions

This research major concerns with the of corrosion on the durability performance of circular SSTT-confined concrete. The following conclusions can be drawn from the study:

- A total of 11 circular SSTT-confined concrete with different prestressing level and corrosion protection were corroded and tested uniaxial compression. Corrosion was simulated through lab-designed impressed current accelerated corrosion technique. Experimental results indicated that circular SSTT-confined concrete indicated its ability to maintain well for its peak strength with slight reduction in deformation ability under low corrosion severity. Compared to uncorroded confined specimens, the reduction in peak strength was as low as 0.94% - 4.65%, whilst the reduction in deformation ability was more obvious for all corroded specimens. It is expected that higher corrosion degree causes higher reduction in peak strength and deformation ability. Corrosion reduced the effective cross-sectional area and decrease of confinement effect on core concrete, which leads to deterioration of peak strength and deformation ability of confined concrete.

- It is as expected that higher prestressing force applied to circular SSTT-confined concrete resulted in higher corrosion degree. Experimental results shows that all corroded specimens with 500 MPa of prestressing level exhibited greater corrosion degree compared to those with 300 MPa of prestressing level. A higher prestressing level on steel strap leads to more significant formation of microcracks on the surface. This provided more site of initiation for chloride ions to penetrate into, which resulted in acceleration for development of corrosion.
- Corrosion protection system including of sacrificial anode corrosion protection and paint coating were applied to circular SSTT-confined concrete. Experimental results shows that the presence of Zn-Al-Cd ingot sacrificial anode and long oil alkyd paint coating (OAP) provided effective protection to the steel strap confinement and successfully reduced the effect of corrosion and aids in preserving the peak strength and deformation ability of confined concrete. In contrast, 6061 aluminum alloy and 99.9% pure magnesium rod were not capable to provide corrosion protection.
- The proposed models for prediction of peak stress and peak strain shows better performance in overall compared to existing models. The models are applicable to circular SSTT-confined concrete under low corrosion severity, provided that thickness loss of steel confinement is known and reduction of yield strength for corroded steel is considered.

Current study only analyzed on uniaxial compression with limited parameters range for corroded circular SSTT-confined concrete. More comprehensive research with expanded range of parameters such as higher corrosion degree, different concrete and steel grade are recommended to be conducted in future research. Performance of corroded SSTT-confined concrete under different loading conditions such as cyclic loading, seismic and others can be considered. In addition, impressed current accelerated corrosion technique adopted in this study generally induced only uniform corrosion, other methods such as salt spray corrosion can be used in future study to simulate corrosive environment that is more similar to actual conditions.

List of Symbol

C_d	Corrosion Degree
D	Diameter of concrete
E	Elastic modulus
f'_c	Cylindrical strength of concrete
f_{co}	Unconfined concrete strength
f_{cc}	Confined concrete strength
f_l	Confining pressure
f_{le}	Effective confining pressure
f'_l	Confining pressure after corrosion
f_y	Yield strength of steel
f'_y	Yield strength of steel after corrosion
f_u	Ultimate strength of steel
F_h	Hoop tension
H	Height of concrete
k_e	Confinement effectiveness ratio for spacing
k_s	Confinement effectiveness ratio for shape
Δm	Mass loss of steel due to corrosion
R	Corner radius of square section
s	Spacing between steel straps
t	Thickness of steel
t_e	Effective thickness of steel after corrosion

Δt	Thickness loss of steel due to corrosion
V	Potential difference
w	Width of steel
σ	Stress
ε	Strain
ε_{cc}	Peak strain of confined concrete
ε_{co}	Peak strain of unconfined concrete
ε_{u}	Ultimate strain of steel

Acknowledgement

References

[1] Moghaddam H, Samadi M, Pilakoutas K, Mohebbi S. Axial compressive behavior of concrete actively confined by metal strips; part A: experimental study. Materials and Structures. 2010;43(10):1369-81. https://doi.org/10.1617/s11527-010-9588-6

[2] Ma C-K, Awang AZ, Omar W, Liang M. Experimental tests on SSTT-confined HSC columns. Magazine of Concrete Research. 2014;66. https://doi.org/10.1680/macr.14.00065

[3] Holmes N, Niall D, O'Shea C. Active confinement of weakened concrete columns. Materials and Structures. 2015;48(9):2759-77. https://doi.org/10.1617/s11527-014-0352-1

[4] Chin C-L, Ma C-K, Awang AZ, Omar W, Kueh ABH. Stress-strain evaluation of steel-strapped high-strength concrete with modified self-regulating end clips. Structural Concrete. 2018;19(4):1036-48. https://doi.org/10.1002/suco.201700134

[5] Mohd Apandi N, Ma C-K, Awang AZ, Omar W. Structural behaviour of pre-damaged RC columns immediate repaired employing pre-tensioned steel straps. Structures. 2021;34:964-78. https://doi.org/10.1016/j.istruc.2021.08.039

[6] Ma C-K, Garcia R, Yung SCS, Awang AZ, Omar W, Pilakoutas K. Strengthening of pre-damaged concrete cylinders using post-tensioned steel straps. Proceedings Of The Institution Of Civil Engineers-Structures And Buildings. 2019;172(10):703-11. https://doi.org/10.1680/jstbu.18.00031

[7] Mohd Apandi N, Ma C-K, Chin C-L, Awang AZ, Omar W. The Effect of Pre-Damaged Level on Repair Damaged Columns by Using Steel Straps Tensioning Technique. International Journal of Engineering & Technology. 2018;7:31. https://doi.org/10.14419/ijet.v7i3.9.15268

[8] Lee H-P, Awang AZ, Omar W. Experimental Investigation on SSTT confined concrete with low lateral pre-tensioning stresses. J Teknol. 2014;69(3):43-50. https://doi.org/10.11113/jt.v69.3142

[9] Di Sarno L, Majidian A, Karagiannakis G. The Effect of Atmospheric Corrosion on Steel Structures: A State-of-the-Art and Case-Study. Buildings. 2021;11(12):571. https://doi.org/10.3390/buildings11120571

[10] Kumar V, Sharma N, Tiwari SK, Kango S. Atmospheric corrosion of materials and their effects on mechanical properties: A brief review. Materials Today: Proceedings. 2021;44:4677-81. https://doi.org/10.1016/j.matpr.2020.10.939

[11] Han L-H, Hou C-C, Wang Q-L. Behavior of circular CFST stub columns under sustained load and chloride corrosion. Journal of Constructional Steel Research. 2014;103:23-36. https://doi.org/10.1016/j.jcsr.2014.07.021

[12] Gao S, Guo L, Zhang S, Peng Z. Performance degradation of circular thin-walled CFST stub columns in high-latitude offshore region. Thin-Walled Structures. 2020;154:106906. https://doi.org/10.1016/j.tws.2020.106906

[13] Gao S, Peng Z, Li X, Chen D. Tests on axial strength of circle CFST stub columns under marine atmosphere in cold region. Construction and Building Materials. 2020;230:117073. https://doi.org/10.1016/j.conbuildmat.2019.117073

[14] Lee H-P, Awang AX, Omar W. Short term durability of steel-strap confined concrete. Jurnal Teknologi. 2016;78. https://doi.org/10.11113/jt.v78.6243

[15] Quadri TW, Akpan ED, Olasunkanmi LO, Fayemi OE, Ebenso EE. 2 - Fundamentals of corrosion chemistry. In: Hussain CM, Verma C, Aslam J, editors. Environmentally Sustainable Corrosion Inhibitors: Elsevier; 2022. p. 25-45. https://doi.org/10.1016/B978-0-323-85405-4.00019-7

[16] 206-1 E. Concrete - Part 1: Specification, performance, production and conformity. 2000.

[17] Standard B. Testing hardened concrete. Compressive Strength of Test Specimens, BS EN. 2009:12390-3.

[18] ISO E. 6892-1: 2019-Metallic materials-Tensile testing-Part 1: Method of test at room temperature (ISO 6892-1: 2019). Brussels, Belgium. 2019.

[19] Chin C-L, Ma C-K, Awang AZ, Omar W, Kueh A. Stress-strain evaluation of steel-strapped high-strength concrete with modified self-regulating end clips. Structural Concrete. 2018;19. https://doi.org/10.1002/suco.201700134

[20] Awang AZ. Stress-strain behaviour of high-strength concrete with lateral pre-tensioning confinement: Universiti Teknologi Malaysia Johor Bahru; 2013.

[21] 8407 I. Corrosion of metals and alloys - Removal of corrosion products from corrosion test specimens. 2021.

[22] Le L, Sofi M, Lumantarna E. The combined effect of stress and corrosion on mild steel. Journal of Constructional Steel Research. 2021;185:106805. https://doi.org/10.1016/j.jcsr.2021.106805

[23] Gu H, Song G, Dhonde H, Mo YL, Yan S. Concrete early-age strength monitoring using embedded piezoelectric transducers. Smart Materials and Structures. 2006;15(6):1837. https://doi.org/10.1088/0964-1726/15/6/038

[24] Moghaddam H, Samadi M, Pilakoutas K. Compressive behavior of concrete actively confined by metal strips, part B: analysis. Materials and Structures. 2010;43(10):1383-96. https://doi.org/10.1617/s11527-010-9589-5

[25] Zhang F, Xia J, Li G, Guo Z, Chang H, Wang K. Degradation of Axial Ultimate Load-Bearing Capacity of Circular Thin-Walled Concrete-Filled Steel Tubular Stub Columns after Corrosion. Materials [Internet]. 2020; 13(3). https://doi.org/10.3390/ma13030795

[26] Sheikh SA, Uzumeri S. Analytical model for concrete confinement in tied columns. Journal of the structural division. 1982;108(12):2703-22. https://doi.org/10.1061/JSDEAG.0006100

[27] Awang AZ, editor Stress-strain behaviour of high-strength concrete with lateral pre-tensioning confinement2013.

[28] Lee H-P, Awang AZ, Omar W. Strength and ductility of high-strength concrete cylinders externally confined with Steel Strapping Tensioning Technique (SSTT). J Teknol. 2014;68(1):109-18. https://doi.org/10.11113/jt.v68.1967

[29] Chin C-L, Ma C-K, Awang AZ, Omar W, Kueh ABH. Stress-strain evaluation of steel-strapped high-strength concrete with modified self-regulating end clips. Structural Concrete. 2018;19(4):1036-48. https://doi.org/10.1002/suco.201700134

[30] Yang Y, Xue Y, Yu Y, Li Y. Research on axial behavior of concrete columns retrofitted with pre-stressed steel strips. Magazine of Concrete Research. 2019;72:1-36. https://doi.org/10.1680/jmacr.18.00107